

Showcasing research from Dr. Kothandaraman and co-workers, Pacific Northwest National Laboratory, Richland, WA, US.

Reactive direct air capture of CO<sub>2</sub> to C-C coupled products using multifunctional materials

A combined sorbent-catalytic material (Fe/K<sub>2</sub>CO<sub>3</sub>/Al<sub>2</sub>O<sub>3</sub>) has been developed for the Integrated Direct Air Capture and Catalytic (iDAC-CAT) process, which converts captured CO<sub>2</sub> from air into valuable C<sub>2</sub><sup>+</sup> products such as olefins. Herein, the proximity between K and Fe was identified as critical for producing C-C coupled products from the captured CO<sub>2</sub>. Initial technoeconomic and life-cycle assessments suggest that the proposed iDAC-CAT technology can considerably lower DAC costs and potentially produce renewable olefins with negative greenhouse gas emissions.

As featured in:



See Jotheeswari Kothandaraman et al., *Green Chem.*, 2024, 26, 8242.



Cite this: *Green Chem.*, 2024, **26**, 8242

# Reactive direct air capture of CO<sub>2</sub> to C–C coupled products using multifunctional materials†

Shazia Sharmin Satter, Johnny Saavedra Lopez, Michael L. Hubbard, Yuan Jiang, Robert A. Dagle and Jotheeswari Kothandaraman \*

Current direct air capture (DAC) approaches require a significant amount of energy for heating CO<sub>2</sub>-sorbed materials for regeneration and for compressing CO<sub>2</sub> for transportation purposes. Rationally designing materials offering both capture and conversion functionalities could enable more energy and cost-efficient DAC and conversion. We have developed a single sorbent-catalytic (non-noble metal) material for the Integrated Direct Air Capture and CATALytic (iDAC-CAT) conversion of captured CO<sub>2</sub> into value-added products. Solid sorbents are integrated with catalytic components to first capture CO<sub>2</sub> from air. Subsequently, captured CO<sub>2</sub>, with renewable H<sub>2</sub> co-feed is converted into olefins and paraffins. To the best of our knowledge, this is the first proof-of-concept demonstration for production of C<sub>2</sub> products such as olefins from captured CO<sub>2</sub>. Among the different sorbent-catalytic materials studied, Fe/K<sub>2</sub>CO<sub>3</sub>/Al<sub>2</sub>O<sub>3</sub> showed the best performance for integrated CO<sub>2</sub> capture and conversion to C<sub>2</sub> products. CO<sub>2</sub> capture capacity of 8.2 wt% was achieved under optimized capture conditions at 25 °C, and a conversion of >70% to paraffins and olefins was achieved at 320–400 °C. The hydrogenation of captured CO<sub>2</sub> was facilitated by the *in situ* formation of Fe<sub>3</sub>O<sub>4</sub> and Fe<sub>5</sub>C<sub>2</sub> species. The proximity between K and Fe was identified to be critical for producing C<sub>2</sub> products from the captured CO<sub>2</sub>. The preliminary technoeconomic and life-cycle assessments suggest that the cost of the DAC can be considerably decreased by adopting the suggested iDAC-CAT technology, while renewable olefins could potentially be produced with negative greenhouse gases emissions.

Received 13th March 2024,

Accepted 13th May 2024

DOI: 10.1039/d4gc01244e

[rsc.li/greenchem](http://rsc.li/greenchem)

## Introduction

Given the increasing CO<sub>2</sub> concentration in the atmosphere, rapid and massive deployment of negative emission technologies (NETs) will be needed to limit global temperature increase to 1.5–2 °C.<sup>1</sup> NETs should be large enough to remove several gigaton quantities of CO<sub>2</sub> from the atmosphere and in this context, DAC is expected to complement other NET options. DAC technologies remove CO<sub>2</sub> from the atmosphere at any location to balance emissions that are unavoidable or technically difficult to avoid.<sup>2</sup> A variety of sorbents are being investigated for CO<sub>2</sub> capture, including physisorbents such as metal–organic frameworks,<sup>3</sup> zeolites,<sup>4,5</sup> and activated carbon,<sup>6</sup> as well as chemisorbents such as amine-functionalized adsorbents that commonly contain polyamines.<sup>7,8</sup> Particularly, chemisorbents are best suited for CO<sub>2</sub> capture from ultra-dilute sources such as air due to strong chemical interactions between CO<sub>2</sub> and sorbents. As a result, chemisorbents are the

subject of extensive studies aimed at understanding and improving their CO<sub>2</sub> adsorption and desorption processes. However, the economic feasibility of large-scale deployment of current DAC systems is uncertain due to high energy input needed for the desorption process (cost estimates are \$200–1000 per tonne CO<sub>2</sub> for DAC compared to \$36–53 per tonne CO<sub>2</sub> for coal-derived flue gas).<sup>9</sup> Thus, innovative use opportunities, including synthetic fuels and chemicals are desired as a means to drive down costs and provide a market for DAC. However, there are no commercial technologies that can economically produce either value-added fuels and chemicals, or solid products for storage using CO<sub>2</sub> captured from air.

The capture of CO<sub>2</sub> and conversion of CO<sub>2</sub> have long been viewed as two independent processes. Recently, the benefits associated with integrating the capture and conversion processes have been realized by the scientific community.<sup>10–13</sup> The direct conversion of captured CO<sub>2</sub> into value-added products (coupled approach) has potential advantages over traditional decoupled CO<sub>2</sub> capture and CO<sub>2</sub> conversion because the coupled approach avoids the energy-intensive sorbent regeneration (CO<sub>2</sub> desorption), compression and transportation steps. Importantly, new reactive pathways for the CO<sub>2</sub> conversion can be realized in the capture media, leading to

Pacific Northwest National Laboratory, Advanced Energy Systems, 902 Battelle Blvd, Richland, WA 99352, USA. E-mail: [jotheeswari.kothandaraman@pnnl.gov](mailto:jotheeswari.kothandaraman@pnnl.gov)

† Electronic supplementary information (ESI) available. See DOI: <https://doi.org/10.1039/d4gc01244e>





higher conversion, selectivity, and reduced cost.<sup>11</sup> For example, typical gas-phase CO<sub>2</sub> hydrogenation to methanol requires high temperatures due to slower kinetics. At high temperature, a competing reaction—the reverse water gas shift reaction—is also favored, which reduces the selectivity and consumes valuable H<sub>2</sub>. On the other hand, in the amine-based capture medium, CO<sub>2</sub> hydrogenation to methanol followed a nontraditional route for conversion to methanol through a formamide intermediate.<sup>14–17</sup> This nontraditional low-temperature methanol synthesis route was made possible by the presence of an amine-based capture solvent medium. However, amine-based aqueous/non-aqueous solvents are not suitable for DAC application due to high volatility, viscosity, and evaporative loss of water under realistic DAC conditions. For DAC, solid sorbents have several benefits (over well-studied liquid sorbents) such as increased adsorption capacities, lower regeneration energy penalties, relative ease of handling, and improved recyclability.<sup>18,19</sup>

Though the feasibility of integrating capture and conversion processes has been shown with liquid capture solvent systems,<sup>11,14,17,20–23</sup> the material design principles are not transferable to solids because unlike liquid systems, the sorbent and catalyst need to be integrated into a single multifunctional material in solids. The solid-state iDAC-CAT approach is limited by the lack of design parameters for this

multifunctional material with the cooperative sorbent and catalytic features to perform both capture and conversion. In traditional DAC approaches, solid or liquid sorbents with low reaction enthalpy, high capture capacity, and rapid kinetics are preferred. The strong binding of CO<sub>2</sub> *via* chemisorption is considered a limitation in traditional DAC approaches due to regeneration requirements. But in the iDAC-CAT approach, the strong binding will be considered an opportunity because the captured CO<sub>2</sub> is undergoing chemical conversion. The strong CO<sub>2</sub> binding will enhance the CO<sub>2</sub> uptake kinetics, which is critical for DAC application.

Solid materials with dual functionalities have been reported for integrated CO<sub>2</sub> capture and conversion to C<sub>1</sub> products such as methane<sup>24–30</sup> and methanol.<sup>31–34</sup> Most of these materials are composed of sorbents (metal oxides and carbonates) and metal catalysts (such as Ru, Ni, and Rh).<sup>35,36</sup> In a first step, the sorbent reacts with CO<sub>2</sub> to form (bi)carbonate and in a second step, (bi)carbonate reacts with hydrogen at high temperature (>300 °C) to form methane. Most of these materials also require high temperature for capture, which is not an economical option.<sup>24,37–39</sup> Amine-functionalized silica and Pd catalyst combinations have been demonstrated to be active for the integrated capture and conversion to methanol.<sup>32,33</sup> Recently, Cu/Zn catalyst and metal carbonate combinations were identified as effective for the reactive capture of CO<sub>2</sub> to methanol.<sup>31,34</sup> While these materials are effective for the formation of C<sub>1</sub> products, the conversion of captured CO<sub>2</sub> to C<sub>2+</sub> products remains a challenge.

In this work, we report how combinations of catalytic components and sorbents can be integrated into a single material that can capture CO<sub>2</sub> from air at ambient conditions, and then convert the captured CO<sub>2</sub> into valuable C<sub>2</sub> products such as olefins. Olefins are building blocks for producing a variety of products including plastics, paints, lubricants, and surfactants. Olefins can also be converted into hard-to-decarbonize jet and diesel fuels.<sup>40</sup> In this work, Fe-based catalytic components were incorporated into the sorbent materials to facilitate the formation of C–C bonds. Upon studying different materials and conditions, we show a proof of concept using Fe/K<sub>2</sub>CO<sub>3</sub>/Al<sub>2</sub>O<sub>3</sub> (Fe/KA) to produce C<sub>2</sub>–C<sub>4</sub> olefins from CO<sub>2</sub> derived from air. We also identified that these materials are effective at converting gas-phase CO<sub>2</sub> to olefins, with olefin to paraffin ratio of 6.9 at 360 °C.

## Results and discussion

### CO<sub>2</sub> capture studies using K<sub>2</sub>CO<sub>3</sub>/Al<sub>2</sub>O<sub>3</sub>

Inorganic chemisorbents are chosen for this study because they are more durable and low-cost materials compared to amine-based sorbents for DAC.<sup>41</sup> The commonly used inorganic chemisorbents for DAC are CaO, MgO, and alkali metal carbonates.<sup>42</sup> Among these sorbents, alkali metal carbonates can perform capture at ambient temperature.<sup>43,44</sup> Alkali metal carbonates are usually dispersed on high-surface-area materials such as Al<sub>2</sub>O<sub>3</sub>, to increase the carbonation rate



**Jotheeswari Kothandaraman**

*Dr Jothi Kothandaraman is a Scientist at the Pacific Northwest National Laboratory (PNNL), one of the US Department of Energy national laboratories. She obtained her Ph.D. in chemistry from the University of Southern California, focusing on catalytically driven reversible hydrogen storage materials. In 2017, she joined PNNL as a postdoctoral researcher, performing research on the catalytic conversion of CO<sub>2</sub>. In 2019, she accepted a*

*full-time Scientist position at PNNL. She is interested in developing green and sustainable chemical processes for fuels and materials. Currently, she is leading projects on the upcycling of CO<sub>2</sub> sourced from both air and flue gas emissions. Dr Kothandaraman holds two US patents and has authored invited book chapters and perspective articles on CO<sub>2</sub> capture and conversion. Dr Kothandaraman's contributions have been recognized with the Phi Kappa Phi Award for Creative and Scholarly Achievements. In 2023, Dr Kothandaraman was elected Fellow of the Royal Society of Chemistry, and she also received the PNNL Laboratory Director's Award for Early Career Exceptional Achievement, also known as the Ronald L. Brodzinski Award. Currently, she serves as an advisory board member for the RSC Sustainability journal.*



of alkali carbonates.<sup>45,46</sup> Based on literature studies conducted on  $K_2CO_3$  loading on various supports, including carbon, alumina, and  $ZrO_2$ , an optimal  $K_2CO_3$  loading between 25–35 wt% on supports was identified for  $CO_2$  capture. The adsorption capacity increases with higher  $K_2CO_3$  loading; however, loading above 35 wt% results in decreased adsorption capacity due to reductions in surface area and pore volume.<sup>47–49</sup> Thus, here 25 wt% of  $K_2CO_3/Al_2O_3$  was synthesized,<sup>50</sup> characterized, and evaluated at 25 °C at different capture conditions to identify suitable conditions for DAC (sections S1.2, 1.3 and 1.4†). As-synthesized  $K_2CO_3/Al_2O_3$  was characterized by BET (Brunauer–Emmett–Teller) analysis. Type IV isotherms with a characteristic hysteresis loop for both  $Al_2O_3$  and  $K_2CO_3/Al_2O_3$  were realized in the BET analysis (shown in Fig. S1A†), indicating that alumina is mesoporous in nature. Impregnation of  $K_2CO_3$  over alumina resulted in a decrease in both surface area and pore volume of the original support, but the average pore sizes were almost comparable as shown in Table S1.† This implies that smaller sizes of  $K_2CO_3$  filled the pores of the mesoporous alumina, confirming the dispersion of  $K_2CO_3$  over the alumina surface.<sup>44</sup>

The effect of pretreatment conditions and water vapor content on the capture performance of the sorbent was studied. The  $K_2CO_3/Al_2O_3$  sorbent was first pretreated at 200 °C for 1 h under  $N_2$  flow ( $100\text{ mL min}^{-1}$ ). The material was then cooled to room temperature and pre-saturated with both 0.5 and 1.0 mol%  $H_2O$  vapor, followed by introduction of 400 ppm of  $CO_2$  (Fig. S2A and S2B†) with  $H_2O$  vapor (0.5 or 1.0 mol%). The amount of  $CO_2$  per g of sorbent adsorbed during both the experiments was calculated from the molar flow concentration profile of  $CO_2$  versus time. For 0.5 mol% of  $H_2O$ ,  $850\text{ }\mu\text{mol g}^{-1}$  of  $CO_2$  was adsorbed, whereas in the case of 1.0 mol% of  $H_2O$ ,  $770\text{ }\mu\text{mol g}^{-1}$  of  $CO_2$  was adsorbed. This indicates that the 0.5 mol% of  $H_2O$  had a slightly higher adsorption capacity, possibly due to the  $K_2CO_3$  phase transition in the presence of excess water.<sup>51</sup>

The effect of saturating the sorbent with water vapor during  $CO_2$  capture was investigated. Here,  $CO_2$  was co-fed with 0.5 mol%  $H_2O$  vapor over the pretreated  $K_2CO_3/Al_2O_3$  as shown in Fig. S3† and compared with the pre-saturated sample (0.5 mol%  $H_2O$  vapor pretreatment). The water vapor co-fed sample shows the highest sorption capacity of 6.5 wt% compared to the water vapor pretreated samples, as shown in Fig. S3.† The amount of  $CO_2$  adsorbed by the 25 wt%  $K_2CO_3/Al_2O_3$  sorbent is ~6.5 wt%, surpassing the amounts reported in the literature, which are 3.6 wt% for  $K_2CO_3/Al_2O_3$  and 4.1 wt% for  $K_2CO_3/Al_2O_3$ -750 ( $Al_2O_3$  heated at 750 °C before  $K_2CO_3$  impregnation) under similar capture conditions, as shown in Table S3.†<sup>52</sup> The increased  $CO_2$  capture capacity could result from the fine dispersion of  $K_2CO_3$  over  $Al_2O_3$ . The X-ray diffraction (XRD) analysis shown in Fig. S1B† illustrates the change in phase composition of the  $K_2CO_3/Al_2O_3$  before and after  $CO_2$  capture at room temperature in the presence of water vapor. For fresh  $K_2CO_3/Al_2O_3$ , the main diffraction peaks were attributed to dawsonite,  $KAlCO_3(OH)_2$ ,  $K_2CO_3$ , and  $\gamma\text{-}Al_2O_3$ . The formation of the dawsonite on the fresh samples

takes place due to the exposure of as-synthesized  $K_2CO_3/Al_2O_3$  to  $CO_2$  in air. This agrees with the Temperature Programmed Desorption (TPD) of the fresh material shown in Fig. S1C,† where the peak at 350 °C is due to the decomposition of the dawsonite.

Thermal decomposition of the  $CO_2$ -captured  $K_2CO_3$  using TPD shown in Fig. S1C† shows two characteristic peaks within 100–200 °C, which is likely due to the decomposition of the species containing bicarbonate,  $K_2CO_3\cdot 2KHCO_3\cdot 1.5H_2O$ , and  $KHCO_3$ . This agrees with the XRD diffraction patterns of the air-captured sorbent. The higher-temperature peak is mainly due to the decomposition of the  $KAlCO_3(OH)_2$ , which was reported to take place between 260 and 320 °C.<sup>44</sup>

As activated carbon (AC) is recognized as a suitable support material for  $CO_2$  capture,  $K_2CO_3/AC$  was synthesized and tested to evaluate its  $CO_2$  capture capacity.<sup>49</sup> Compared to  $K_2CO_3/Al_2O_3$ , the capture capacity of  $K_2CO_3/AC$  was 1.3 times lower, as shown in Fig. S4.† Due to the superior capture performance of  $K_2CO_3/Al_2O_3$  under the optimized reaction conditions,  $K_2CO_3/Al_2O_3$  was chosen as the sorbent material for the integrated capture and conversion studies.

### Conversion of captured $CO_2$ to $C_1$ and $C_2$ products

The direct conversion of captured  $CO_2$  from air or concentrated point sources to  $C_1$  products such as methane, methanol, and CO has been effectively demonstrated in earlier studies.<sup>24–26,29–31,34,53</sup> However, due to the high energy barrier of C–C coupling reactions, conversion of captured  $CO_2$  to  $C_{2+}$  products is still a challenge. In the literature, combining the endothermic reverse water gas shift (RWGS) ( $CO_2 + H_2 \rightarrow CO + H_2O$ ) reaction with the exothermic Fischer–Tropsch (FTS) ( $CO + H_2 \rightarrow C_xH_y$ ) reaction has been identified as one of the strategies for converting concentrated streams of  $CO_2$  and  $H_2$  in the gas phase to  $C_{2+}$  products.<sup>54</sup> Particularly, potassium (alkali metal) modified Fe-based catalysts are known to promote carbon-chain growth in the gas-phase  $CO_2$  hydrogenation reactions.<sup>55–58</sup> We hypothesized that by combining the Fe-based catalysts and potassium-based sorbents the captured  $CO_2$  can be directly converted to  $C_{2+}$  products, bypassing the energy-intensive  $CO_2$  regeneration and compression steps. Additionally, alkali modification of metals can potentially develop optimal electronics that allow the selective formation of olefins by decreasing the reactivity of adsorbed H species.<sup>59,60</sup> To test our hypothesis, we synthesized different combinations of iron and  $K_2CO_3/Al_2O_3$  based sorbent-catalytic materials and evaluated the capture and conversion performance of these synthesized materials.

**$Fe_2O_3$ – $K_2CO_3/Al_2O_3$ .** A physical mixture of  $Fe_2O_3$  and  $K_2CO_3$  has been reported to be effective for converting  $CO_2$  into  $C_2$ – $C_4$  olefins with approximately 31% selectivity *via* a tandem mechanism.<sup>56</sup> The addition of  $K_2CO_3$  is the key for promoting the formation of CO (*via* potassium bicarbonate and potassium formate intermediates), which gets converted into olefins and paraffins in the presence of iron oxide and iron carbide phases at 350 °C. Based on this study, we evaluated a physical mixture of  $Fe_2O_3$ – $K_2CO_3/Al_2O_3$  ( $Fe_2O_3$ –KA). The  $Fe_2O_3$ –KA was



prepared as mentioned in section S1.2† and pretreated at 400 °C under H<sub>2</sub> flow (60 mL min<sup>-1</sup>) for 5 h to convert Fe<sub>2</sub>O<sub>3</sub> to Fe nanoparticles.

CO<sub>2</sub> capture was performed with 400 ppm of CO<sub>2</sub> (1200 mL min<sup>-1</sup>) and 0.5 mol% of H<sub>2</sub>O at 25 °C. The capture performance was compared with K<sub>2</sub>CO<sub>3</sub>/Al<sub>2</sub>O<sub>3</sub>, which was activated under similar conditions. Under this condition, ~100% of the K<sub>2</sub>CO<sub>3</sub> was utilized during CO<sub>2</sub> capture in the case of K<sub>2</sub>CO<sub>3</sub>/Al<sub>2</sub>O<sub>3</sub>, whereas in the case of Fe<sub>2</sub>O<sub>3</sub>-KA, only 81% of the K<sub>2</sub>CO<sub>3</sub> was utilized in CO<sub>2</sub> capture, as shown in Table S2.† High-temperature pretreatment enhanced the capture capacity through the dawsonite decomposition reaction.<sup>44</sup> Then, hydrogenation of the captured CO<sub>2</sub> was performed under hydrogen pressure of 1.0 MPa at 320 °C (hold for 2.5 h) and 360 °C (hold for 2 h) at a ramp rate of 5 °C min<sup>-1</sup> under H<sub>2</sub> flow (60 mL min<sup>-1</sup>). This resulted in desorption of CO<sub>2</sub> with no detectable amount of hydrogenated CO<sub>2</sub>-derived products. Most of the CO<sub>2</sub> was released at ~320 °C, suggesting that dawsonite is the major species formed during CO<sub>2</sub> capture.

**K<sub>2</sub>CO<sub>3</sub>/Fe/C and K<sub>2</sub>CO<sub>3</sub>/Fe/C/Al<sub>2</sub>O<sub>3</sub>.** Sun *et al.* showed that the use of potassium-promoter-modified Fe/C catalysts can

increase olefin selectivity in CO<sub>2</sub> hydrogenation.<sup>57</sup> Fe/C was synthesized by the hydrothermal method (section S1.2 in ESI†). K<sub>2</sub>CO<sub>3</sub>/Fe/C was formed by impregnating K<sub>2</sub>CO<sub>3</sub> (25 wt%) on the Fe/C catalyst. The synthesized material was pretreated at 400 °C under H<sub>2</sub> flow for 10 h to ensure carbide formation before CO<sub>2</sub> capture and conversion studies.<sup>57</sup> CO<sub>2</sub> capture was performed by following the standard capture procedure mentioned in section S1.4.† The capture profile is shown in Fig. 1A. In the first 50 min, there was an induction period after which the CO<sub>2</sub> capture breakpoint started. The initial delay in the capture could either be due to physical adsorption of the CO<sub>2</sub> occupying the macropores of the materials or because the material surface was not immediately saturated with water vapor, which is necessary to start the carbonation reaction. The total CO<sub>2</sub> captured in 4 hours by this material typically ranges between 600 and 700 μmol g<sup>-1</sup>, which is ~2 times lower than that of K<sub>2</sub>CO<sub>3</sub>/Al<sub>2</sub>O<sub>3</sub> (see Table 1).

As shown in Fig. 1B, conversion of the captured CO<sub>2</sub> was carried out with H<sub>2</sub> feed at different temperatures. When the temperature was increased from room temperature (capture) to 320 °C (conversion) some unreacted CO<sub>2</sub> began to desorb.

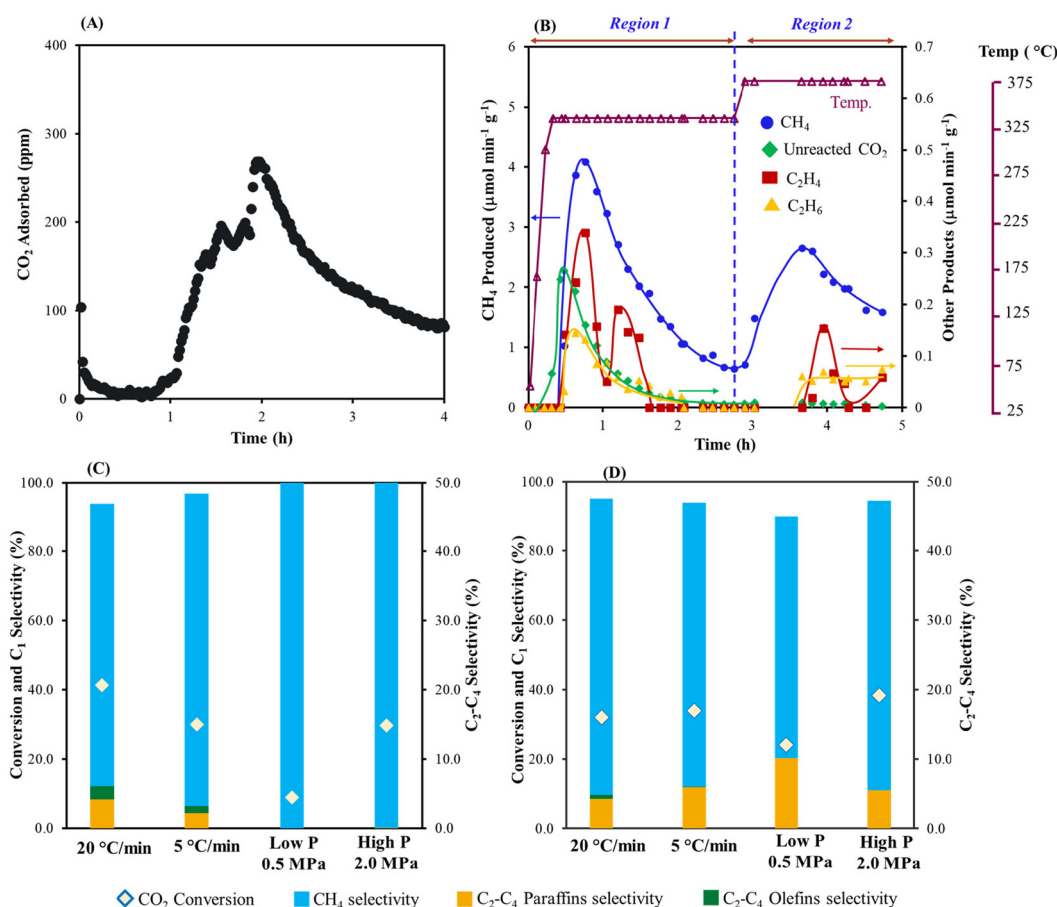


**Fig. 1** (A) CO<sub>2</sub> capture profile over K<sub>2</sub>CO<sub>3</sub>/Fe/C at 25 °C, (B) hydrogenation profile of the captured CO<sub>2</sub> (at heating rate of 20 °C min<sup>-1</sup>), (C) comparison of the CO<sub>2</sub> conversion and selectivity of products formed in Region 1, at 320 °C, and (D) comparison of the CO<sub>2</sub> conversion and selectivity of the products formed in Region 2, at 360 °C. Amount of material: 2 g; pretreatment conditions: H<sub>2</sub> = 60 mL min<sup>-1</sup>, 400 °C, 10 h; CO<sub>2</sub> capture conditions: CO<sub>2</sub> = 400 ppm in N<sub>2</sub> (flow rate = 1200 mL min<sup>-1</sup>), H<sub>2</sub>O vapor = 0.5 mol%, 25 °C, 4 h; hydrogenation: H<sub>2</sub> = 60 mL min<sup>-1</sup>, 1.0 MPa, 320 °C for 2.5 h (5 °C min<sup>-1</sup>), followed by heating to 360 °C (5 °C min<sup>-1</sup>) for 2 h. The selectivity of CO is <5% during the hydrogenation.



**Table 1** Comparison of the physicochemical properties, CO<sub>2</sub> capture and catalytic activity

Entry	Materials	Physical properties			CO <sub>2</sub> capture		Catalytic activity				
		SA (m <sup>2</sup> g <sup>-1</sup> )	PV (cm <sup>3</sup> g <sup>-1</sup> )	Average diameter (nm)	(μmol g <sup>-1</sup> )	(wt%)	CO <sub>2</sub> conv. (%)	CH <sub>4</sub> sel (%)	C <sub>2</sub> –C <sub>4</sub> paraffins sel (%)	C <sub>2</sub> –C <sub>4</sub> olefins sel (%)	C <sub>5</sub> + sel (%)
1	Fe/C	33.16	0.4008	— <sup>c</sup>	N/A	N/A	N/A	N/A	N/A	N/A	N/A
2	Al <sub>2</sub> O <sub>3</sub>	182.4	0.6001	11.4	N/A	N/A	N/A	N/A	N/A	N/A	N/A
3	K <sub>2</sub> CO <sub>3</sub> /Al <sub>2</sub> O <sub>3</sub>	99.19	0.3262	10.09	1862	8.2	N/A	N/A	N/A	N/A	N/A
4	K <sub>2</sub> CO <sub>3</sub> /Fe/C <sup>a</sup>	—	—	—	600–700	2.6–3.1	30.0	96.8	2.2	1.0	0.0
5	K <sub>2</sub> CO <sub>3</sub> /Fe/C <sup>b</sup>	—	—	—	—	—	41.4	93.9	4.1	2.0	0.0
6	K <sub>2</sub> CO <sub>3</sub> /Fe/C/Al <sub>2</sub> O <sub>3</sub> <sup>a</sup>	29.23	0.2476	8.95	1223	5.4	30.5	83.2	8.6	7.3	0.9

Pretreatment conditions for materials: H<sub>2</sub> = 60 mL min<sup>-1</sup>, 400 °C, 5 h (entry 3) and 10 h (for entries 4–6); CO<sub>2</sub> capture conditions: CO<sub>2</sub> = 400 ppm in N<sub>2</sub> (flow rate = 1200 mL min<sup>-1</sup>), H<sub>2</sub>O vapor = 0.5 mol%, 25 °C, 4 h; hydrogenation: H<sub>2</sub> = 60 mL min<sup>-1</sup>, 1.0 MPa, 320 °C for 2.5 h (5 °C min<sup>-1</sup>).

<sup>a</sup> Heating rate at 5 °C min<sup>-1</sup> during hydrogenation of captured CO<sub>2</sub>. <sup>b</sup> Heating rate of 20 °C min<sup>-1</sup> during hydrogenation of captured CO<sub>2</sub>.

<sup>c</sup> Average diameter is not given due to low surface area.

Along with CO<sub>2</sub>, CH<sub>4</sub> also formed and was the highest when the temperature reached 320 °C as shown in Fig. 1B. C<sub>2</sub>H<sub>4</sub> and C<sub>2</sub>H<sub>6</sub> were also produced at Region 1 (at 320 °C, 2.5 h). Further increasing the temperature to 360 °C resulted in additional CH<sub>4</sub> production along with small amounts of ethylene and ethane (Fig. 1D). Overall, ~74% of the total captured CO<sub>2</sub> was converted to C<sub>1</sub> and C<sub>2</sub> products with ~94.4% selectivity to methane, 4.2% selectivity to ethane, and 1.4% selectivity to ethene. To the best of our knowledge, this is the first demonstration for conversion of captured CO<sub>2</sub> (air derived) to C<sub>1</sub> and C<sub>2</sub> based products in the presence of an Fe-based catalyst. Besides the formation of olefins, which are the target products, the production of renewable methane from the captured CO<sub>2</sub> is also advantageous. This presents an alternative pathway for generating synthetic natural gas, and its utilization in existing infrastructure could lead to a lower carbon footprint. There were no detectable amounts of higher olefins or paraffins formed. Decreasing the heating rate from 20 to 5 °C min<sup>-1</sup> decreased the overall conversion of CO<sub>2</sub> along with a decrease in olefin selectivity at 320 °C (Fig. 1C). Increasing the hydrogen pressure further increased the selectivity to methane with a

decrease in the conversion of the captured CO<sub>2</sub> (see Fig. 1C and D).

A decrease in CO<sub>2</sub> capture with K<sub>2</sub>CO<sub>3</sub>/Fe/C compared to K<sub>2</sub>CO<sub>3</sub>/Al<sub>2</sub>O<sub>3</sub> is likely due to the smaller surface area of Fe/C (33.16 m<sup>2</sup> g<sup>-1</sup>), which results in larger K<sub>2</sub>CO<sub>3</sub> particles (Table 1). A lower CO<sub>2</sub> loading could inhibit C–C bond formation because there are fewer carbons. To increase the surface area and eventually improve the capture performance, K<sub>2</sub>CO<sub>3</sub>/Fe/C/Al<sub>2</sub>O<sub>3</sub> was synthesized *via* the wet impregnation method, as discussed in section S1.2,<sup>†</sup> and the adsorption capacity was compared with that of K<sub>2</sub>CO<sub>3</sub>/Al<sub>2</sub>O<sub>3</sub> and K<sub>2</sub>CO<sub>3</sub>/Fe/C under similar capture conditions. The capture performance was significantly improved after the addition of Al<sub>2</sub>O<sub>3</sub>. The K<sub>2</sub>CO<sub>3</sub>/Fe/C/Al<sub>2</sub>O<sub>3</sub> captured ~1220 μmol g<sup>-1</sup> of CO<sub>2</sub> (vs. 600–700 μmol g<sup>-1</sup> of CO<sub>2</sub> for K<sub>2</sub>CO<sub>3</sub>/Fe/C) (Fig. 2A). This difference can be explained from the BET results of the support over which K<sub>2</sub>CO<sub>3</sub> was impregnated. The BET isotherms of three materials are shown in Fig. 3A. Dispersion of K<sub>2</sub>CO<sub>3</sub> on Al<sub>2</sub>O<sub>3</sub> retained the mesoporosity of the support and showed a type IV isotherm despite a decrease in the surface area as shown in Table 1. The isotherm of Fe/C is a type II isotherm with no pro-

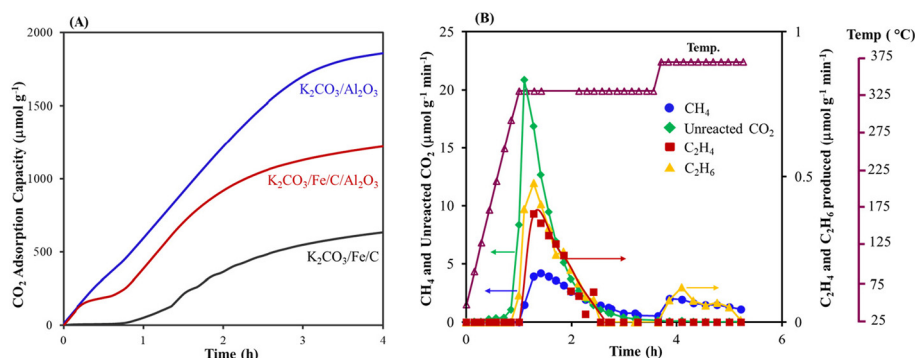


**Fig. 2** (A) Comparison of the CO<sub>2</sub> adsorption capacity of K<sub>2</sub>CO<sub>3</sub> on various materials pretreated at 400 °C under H<sub>2</sub> flow, and (B) hydrogenation of the captured CO<sub>2</sub> over K<sub>2</sub>CO<sub>3</sub>/Fe/C/Al<sub>2</sub>O<sub>3</sub> at 320 and 360 °C. Amount of material: 2 g; pretreatment conditions: H<sub>2</sub> = 60 mL min<sup>-1</sup>, 400 °C, 5 h (K<sub>2</sub>CO<sub>3</sub>/Al<sub>2</sub>O<sub>3</sub>) and 10 h (K<sub>2</sub>CO<sub>3</sub>/Fe/C/Al<sub>2</sub>O<sub>3</sub> and K<sub>2</sub>CO<sub>3</sub>/Fe/C); CO<sub>2</sub> capture conditions: CO<sub>2</sub> = 400 ppm in N<sub>2</sub> (flow rate = 1200 mL min<sup>-1</sup>), H<sub>2</sub>O vapor = 0.5 mol%, 25 °C, 4 h; hydrogenation: H<sub>2</sub> = 60 mL min<sup>-1</sup>, 1.0 MPa, 320 °C for 2.5 h (5 °C min<sup>-1</sup>), followed by heating to 360 °C (5 °C min<sup>-1</sup>) for 2 h. The selectivity of CO is <5% during the hydrogenation.





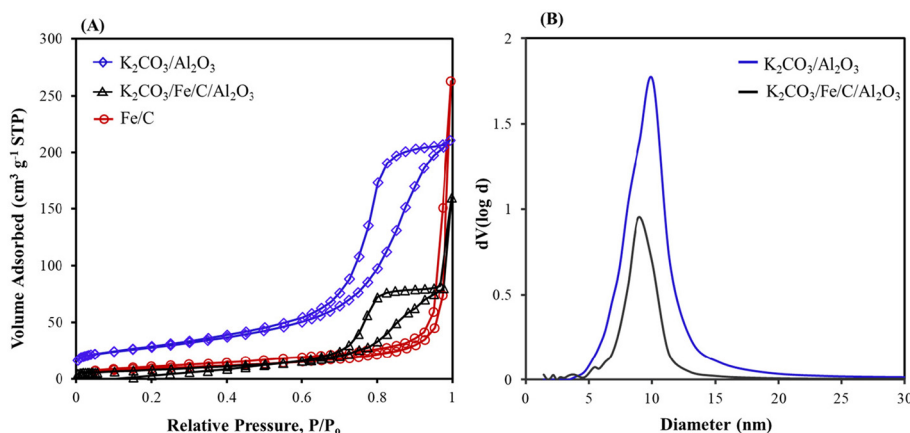


**Fig. 3** (A) Nitrogen adsorption-desorption isotherms of K<sub>2</sub>CO<sub>3</sub>/Al<sub>2</sub>O<sub>3</sub>, K<sub>2</sub>CO<sub>3</sub>/Fe/C/Al<sub>2</sub>O<sub>3</sub>, and Fe/C and (B) Barrett-Joyner-Halenda (BJH) curves for K<sub>2</sub>CO<sub>3</sub>/Al<sub>2</sub>O<sub>3</sub>, and K<sub>2</sub>CO<sub>3</sub>/Fe/C/Al<sub>2</sub>O<sub>3</sub>.

nounced hysteresis loop, showing that the material is either non-porous or microporous. The surface area is very low compared to the Al<sub>2</sub>O<sub>3</sub> support and has no pores, as shown in Table 1. Therefore, the impregnation of K<sub>2</sub>CO<sub>3</sub> could have formed larger particles on Fe/C, leading to lower CO<sub>2</sub> capture.<sup>49</sup> Due to the presence of the Al<sub>2</sub>O<sub>3</sub> pores, K<sub>2</sub>CO<sub>3</sub> was well dispersed over a mixture of high-surface-area, mesoporous Al<sub>2</sub>O<sub>3</sub> and non-porous Fe/C. This led to higher CO<sub>2</sub> capture for K<sub>2</sub>CO<sub>3</sub>/Fe/C/Al<sub>2</sub>O<sub>3</sub> compared to only K<sub>2</sub>CO<sub>3</sub>/Fe/C, as shown in Table 1.

With the improvement in capture performance, the CO<sub>2</sub> captured in K<sub>2</sub>CO<sub>3</sub>/Fe/C/Al<sub>2</sub>O<sub>3</sub> was converted *in situ* (Fig. 2B shows the conversion profile of captured CO<sub>2</sub>). A comparison of the conversion activities of K<sub>2</sub>CO<sub>3</sub>/Fe/C and K<sub>2</sub>CO<sub>3</sub>/Fe/C/Al<sub>2</sub>O<sub>3</sub> is shown in Table 1. Interestingly, the C<sub>2</sub>–C<sub>4</sub> olefin selectivity significantly improved to 7.3% in the case of K<sub>2</sub>CO<sub>3</sub>/Fe/C/Al<sub>2</sub>O<sub>3</sub>. The improved C–C coupled products formation could be because of the relatively high CO<sub>2</sub> loading. In addition, a small amount of C<sub>5+</sub> products (~1%) was also detected. Increasing the hydrogenation temperature to 360 °C increased the conversion and selectivity further to methane. Increased methane formation at higher temperature could be due to a decrease in the chain growth probability of the

Anderson-Schultz-Flory product distribution that governs the FTS reaction.<sup>61</sup> Alternatively, it could be due to less carbon (*i.e.*, captured CO<sub>2</sub>) content on the material, which could prevent C–C formation.

**Fe/K<sub>2</sub>CO<sub>3</sub>/Al<sub>2</sub>O<sub>3</sub> and Fe-Co/K<sub>2</sub>CO<sub>3</sub>/Al<sub>2</sub>O<sub>3</sub>.** Because the physical mixture of Fe<sub>2</sub>O<sub>3</sub>–K<sub>2</sub>CO<sub>3</sub>/Al<sub>2</sub>O<sub>3</sub> formed no CO<sub>2</sub> hydrogenation products, we prepared Fe/K<sub>2</sub>CO<sub>3</sub>/Al<sub>2</sub>O<sub>3</sub> (Fe/KA) and Fe-Co/K<sub>2</sub>CO<sub>3</sub>/Al<sub>2</sub>O<sub>3</sub> (Fe-Co/KA) (by incipient wetness impregnation of Fe and Co salts on K<sub>2</sub>CO<sub>3</sub>/Al<sub>2</sub>O<sub>3</sub>) to improve the cooperativity between Fe and K to produce C–C coupled products. After pretreating these materials at 400 °C for 5 h under H<sub>2</sub> flow, the CO<sub>2</sub> capture was performed under standard conditions (400 ppm of CO<sub>2</sub>, 0.5 mol% of H<sub>2</sub>O vapor, 25 °C, 4 h). The Fe-Co/KA captured 1970 μmol g<sup>−1</sup> of CO<sub>2</sub>, which is almost similar to K<sub>2</sub>CO<sub>3</sub>/Al<sub>2</sub>O<sub>3</sub> (pretreated at 400 °C), showing that the addition of the catalytic component (Fe) had no impact on the capture performance. Hydrogenation of the captured CO<sub>2</sub> using Fe-Co/KA was carried out at two different temperature ramp rates, 5 and 20 °C min<sup>−1</sup>. Increasing the heating rate decreased the CO<sub>2</sub> conversion to value-added products with no significant impact on product distribution, as shown in Table 2.

**Table 2** Comparison of CO<sub>2</sub> capture and conversion performance for Fe-Co/KA and Fe/KA at 320 °C

	Heating rate (°C min <sup>−1</sup> )	CO <sub>2</sub> captured (μmol g <sup>−1</sup> )	CO <sub>2</sub> conv. (%)	Selectivity to hydrocarbons		
				CH <sub>4</sub> sel (%)	C <sub>2</sub> –C <sub>4</sub> paraffins sel (%)	C <sub>2</sub> –C <sub>4</sub> olefins sel (%)
Fe-Co/KA	5	1970	21.3	88.3	5.1	6.7
	20	1970	12.0	86.8	8.3	4.9
Fe/KA	5	1645	22.4	79.7	8.9	11.4
Fe/KA <sup>a</sup>	5	1525	18.1	81.9	6.6	11.5
Fe/KA (H <sub>2</sub> /CO pretreated) <sup>b</sup>	5	1659	24.5	72.1	11.2	16.7

Amount of material: 2 g; pretreatment conditions: H<sub>2</sub> = 60 mL min<sup>−1</sup>, 400 °C, 5 h; CO<sub>2</sub> capture conditions: CO<sub>2</sub> = 400 ppm in N<sub>2</sub> (flow rate = 1200 mL min<sup>−1</sup>), H<sub>2</sub>O vapor = 0.5 mol%, 25 °C, 4 h; hydrogenation: H<sub>2</sub> = 60 mL min<sup>−1</sup>, 1.0 MPa, 320 °C for 2.5 h (5 °C min<sup>−1</sup>). The selectivity of CO is <5% during the hydrogenation. <sup>a</sup> CO<sub>2</sub> capture conditions: CO<sub>2</sub> = 430 ppm CO<sub>2</sub> (in 78% nitrogen, 21% oxygen and <1% other gases).

<sup>b</sup> Pretreatment conditions: H<sub>2</sub>/CO (2 : 1) = 60 mL min<sup>−1</sup>, 400 °C, 3 h, followed by H<sub>2</sub> = 60 mL min<sup>−1</sup>, 400 °C, 5 h.



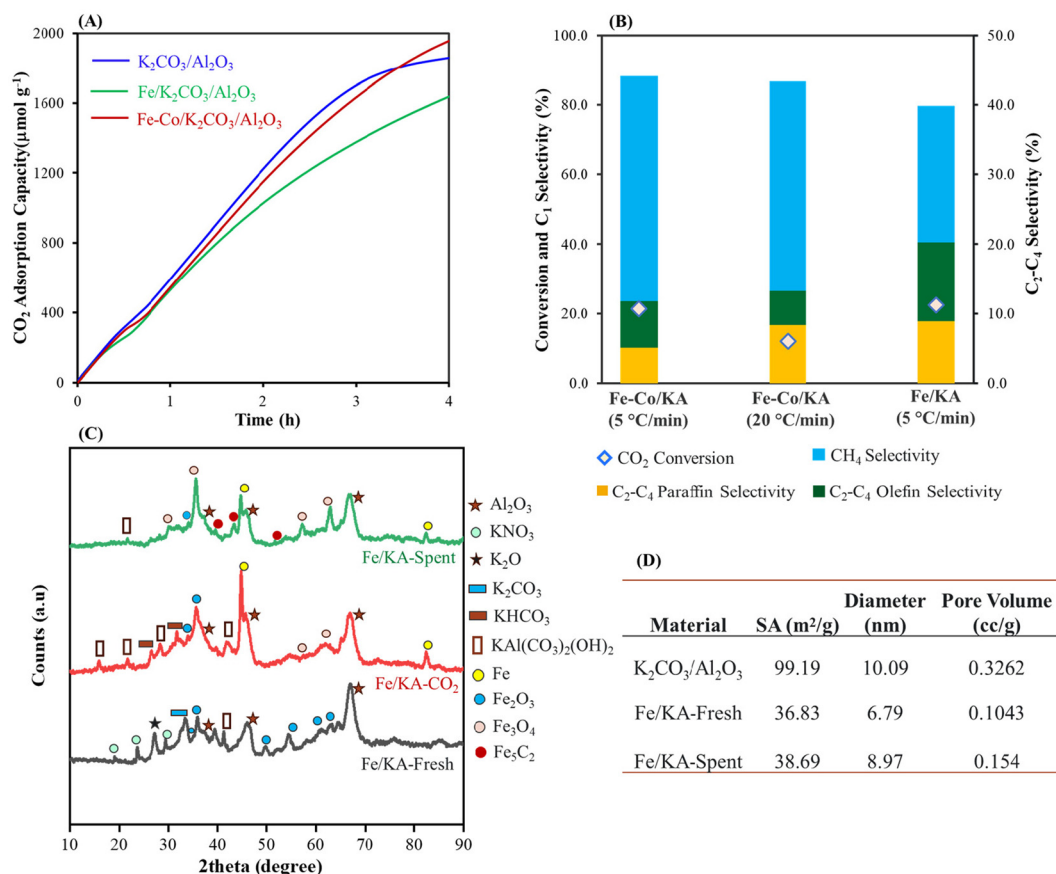


**Fig. 4** (A) Comparison of CO<sub>2</sub> adsorption capacity of K<sub>2</sub>CO<sub>3</sub>/Al<sub>2</sub>O<sub>3</sub>, Fe-Co/K2CO3/Al2O3 and Fe/K2CO3/Al2O3, (B) comparison of hydrogenation of Fe-Co/K2CO3/Al2O3 with different heating rates and Fe/K2CO3/Al2O3 (C) X-ray diffraction patterns of fresh, CO<sub>2</sub> captured and spent Fe/K2CO3/Al2O3, and (D) physicochemical properties of the K<sub>2</sub>CO<sub>3</sub>/Al<sub>2</sub>O<sub>3</sub> and Fe/K2CO3/Al2O3 materials. Amount of material: 2 g; pretreatment conditions: H<sub>2</sub> = 60 mL min<sup>-1</sup>, 400 °C, 5 h; CO<sub>2</sub> capture conditions: CO<sub>2</sub> = 400 ppm in N<sub>2</sub> (flow rate = 1200 mL min<sup>-1</sup>), H<sub>2</sub>O vapor = 0.5 mol%, 25 °C, 4 h; hydrogenation: H<sub>2</sub> = 60 mL min<sup>-1</sup>, 1.0 MPa, 320 °C for 2.5 h (5 °C min<sup>-1</sup>). The selectivity of CO is <5% during the hydrogenation.

The Fe/K2CO3/Al2O3 captured ~1600 μmol g<sup>-1</sup> of CO<sub>2</sub> at our standard capture conditions as shown in Fig. 4A. The hydrogenation results are shown in Fig. S5A† and Table 2. At 320 °C, C<sub>2</sub>-C<sub>4</sub> olefins and paraffins started forming accompanied with the formation of CH<sub>4</sub>. The highest olefin selectivity of ~11.4% was obtained with a CO<sub>2</sub> conversion of 22.4% as shown in Fig. 4B. Next, to understand the effect of oxygen on the capture and conversion, CO<sub>2</sub> capture was performed with real air (430 ppm CO<sub>2</sub> containing 21% oxygen) using Fe/K2CO3/Al2O3, which captured ~1500 μmol g<sup>-1</sup> of CO<sub>2</sub>. After the CO<sub>2</sub> capture, the material was purged with N<sub>2</sub> for 10 min to remove air. The subsequent hydrogenation produced C<sub>2</sub>-C<sub>4</sub> olefins with a selectivity of 11.5% and a CO<sub>2</sub> conversion of 18.1%, suggesting that the presence of oxygen during capture did not significantly affect the conversion and selectivity.

The BET isotherm shows that the mesoporosity of the K<sub>2</sub>CO<sub>3</sub>/Al<sub>2</sub>O<sub>3</sub> is still maintained after impregnation of Fe particles (Fig. S5B†). Upon impregnating Fe, the surface area decreased from 99.19 (for K<sub>2</sub>CO<sub>3</sub>/Al<sub>2</sub>O<sub>3</sub>) to 36.83 m<sup>2</sup> g<sup>-1</sup> and the diameter of the mesopores decreased to 6.79 nm, confirming the formation of Fe particles inside the mesopores (Fig. 4D).

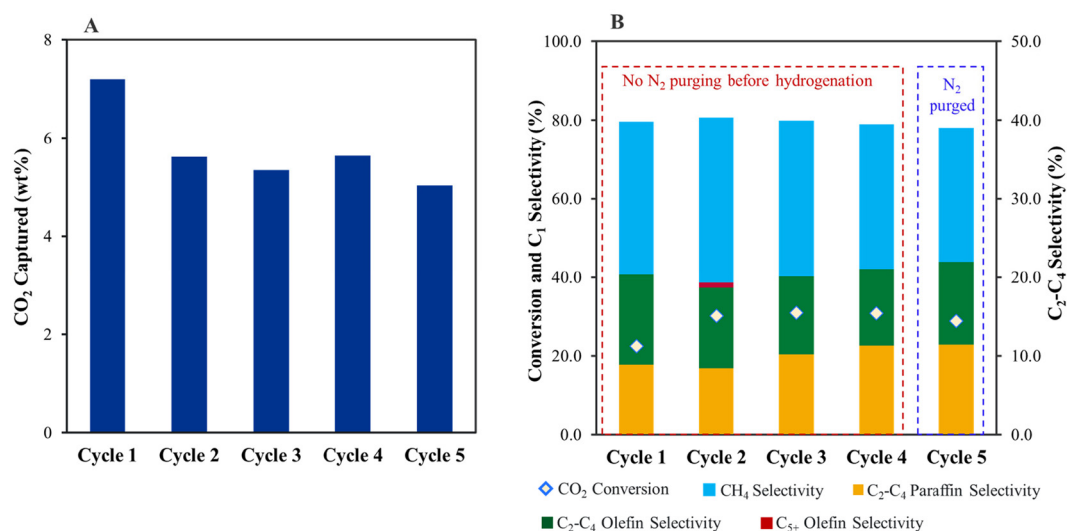
The average pore size of the spent Fe/K2CO3/Al2O3 material (after hydrogenation) increased compared to the fresh material along with slight increase in the pore volume and surface area. This shows that after the hydrogenation, more dispersed particles were formed. This could be due to the formation of Fe<sub>5</sub>C<sub>2</sub> and Fe<sub>3</sub>O<sub>4</sub> particles during the high-temperature hydrogenation.

Fig. 4C shows wide-angle XRD of the fresh Fe/K2CO3/Al2O3, CO<sub>2</sub> captured Fe/K2CO3/Al2O3 and spent (after hydrogenation) Fe/K2CO3/Al2O3. In the fresh sample, diffraction peaks corresponding to KNO<sub>3</sub>, dawsonite, and Fe<sub>2</sub>O<sub>3</sub> particles were evident. XRD of the CO<sub>2</sub>-captured Fe/K2CO3/Al2O3 material shows peaks for KHCO<sub>3</sub> and dawsonite along with some Fe<sub>2</sub>O<sub>3</sub> and Fe particles. The Fe particles could form from Fe<sub>2</sub>O<sub>3</sub> due to hydrogenation with H<sub>2</sub> at high temperature.<sup>62</sup> The spent (after hydrogenation) Fe/K2CO3/Al2O3 shows peaks for Fe<sub>5</sub>C<sub>2</sub> along with Fe<sub>3</sub>O<sub>4</sub>, which were formed during hydrogenation of the captured CO<sub>2</sub>. The formation of these dispersed particles resulted in an increase of pore volume and of the average pore size of the material. The formation of the Fe<sub>5</sub>C<sub>2</sub> phase shows the carburization of Fe<sub>3</sub>O<sub>4</sub> particles.

The spent Fe/K2CO3/Al2O3 after the first cycle of capture and hydrogenation was reused to study the robustness of these materials







**Fig. 5** (A) CO<sub>2</sub> capture and (B) hydrogenation of captured CO<sub>2</sub> over five cycles using Fe/KA. Fe/KA: 2 g, pretreatment conditions: H<sub>2</sub> = 60 mL min<sup>-1</sup>, 400 °C, 5 h; CO<sub>2</sub> capture conditions: CO<sub>2</sub> = 400 ppm in N<sub>2</sub> (flow rate = 1200 mL min<sup>-1</sup>), H<sub>2</sub>O vapor = 0.5 mol%, 25 °C, 4 h; hydrogenation: H<sub>2</sub> = 60 mL min<sup>-1</sup>, 1.0 MPa, 320 °C for 2.5 h (5 °C min<sup>-1</sup>) followed by heating to 400 °C (5 °C min<sup>-1</sup>) for 2.5 h to mimic the pretreatment conditions. For cycle 5, the spent catalyst was purged with N<sub>2</sub> (30 mL min<sup>-1</sup>) for 1 h before hydrogenation. The selectivity of CO is <5% during the hydrogenation.

(Fig. 5). The capture capacity was reduced in the second cycle to 1276 μmol g<sup>-1</sup> (5.6 wt CO<sub>2</sub>%) compared to 1645 μmol g<sup>-1</sup> (7.4 wt CO<sub>2</sub>%) in the first cycle. However, the capture performance was steady in the subsequent third (5.4 wt%), fourth (5.6 wt%), and fifth (~5.03 wt%) cycles. The drop in the capture capacity could be because of the presence of K<sub>2</sub>O in the fresh Fe/KA, which consumed CO<sub>2</sub> from air to form K<sub>2</sub>CO<sub>3</sub>. A similar drop in the capture capacity was observed between the first (6.5 wt% CO<sub>2</sub>) and second cycles (5.3 wt% CO<sub>2</sub>) for K<sub>2</sub>CO<sub>3</sub>/Al<sub>2</sub>O<sub>3</sub> (Table S3†). However, in this case (K<sub>2</sub>CO<sub>3</sub>/Al<sub>2</sub>O<sub>3</sub>), the drop in performance could be because the low-temperature pretreatment conditions (at 200 °C for 1 h) prevented the conversion of dawsonite back to K<sub>2</sub>CO<sub>3</sub>. Prior to hydrogenation during the fifth cycle, the CO<sub>2</sub> captured material was purged with N<sub>2</sub> flow for 1 h to quantify physisorbed CO<sub>2</sub> content. Only trace amounts of CO<sub>2</sub> were released during the N<sub>2</sub> purge, and subsequent hydrogenation showed consistent conversion and selectivity to products, demonstrating that the material is stable for at least five cycles.

To understand the effect of the CO<sub>2</sub>:H<sub>2</sub> ratio and reaction temperature on the product distribution and conversion, the

gas-phase hydrogenation studies were performed with Fe/KA using 1:3 and 1:10 ratios of CO<sub>2</sub>:H<sub>2</sub>. The conversion results for the Fe/KA at 320 °C and 360 °C are shown in Tables 3 and 4, along with Fig. 6. At 320 °C, in the case of the 1:10 ratio of CO<sub>2</sub>/H<sub>2</sub>, the selectivity to C<sub>2</sub>-C<sub>4</sub> paraffins was higher compared to DAC and 1:3 ratio of CO<sub>2</sub>/H<sub>2</sub> studies. The O/P (olefin/paraffin) ratio selectivity to C<sub>2</sub>-C<sub>4</sub> olefins was not significantly altered by the CO<sub>2</sub>/H<sub>2</sub> ratio at 320 °C. In addition to C<sub>2-4</sub> products, C<sub>5+</sub> products were detected by gas chromatography in the case of 1:3 ratio of CO<sub>2</sub>/H<sub>2</sub>. The reaction temperature played a significant role in O/P selectivity and CO<sub>2</sub> conversion. The CO<sub>2</sub> conversion was 66% and 15% for 1:10 and 1:3 ratios of CO<sub>2</sub>/H<sub>2</sub>, respectively, at 360 °C (Table 4). High olefin selectivity and O/P (olefin/paraffin) ratios were achieved for 1:3 ratio of CO<sub>2</sub>/H<sub>2</sub> at 360 °C. In addition, the CO selectivity depends on the reaction temperature and the CO<sub>2</sub>:H<sub>2</sub> ratio. As shown in Tables 3 and 4, a higher temperature (*i.e.*, 360 °C) and lower CO<sub>2</sub> concentrations significantly reduced the CO selectivity, suggesting that the reaction is proceeding *via* the CO intermediate.

**Table 3** Comparison of hydrogenation of captured CO<sub>2</sub> with gas-phase CO<sub>2</sub> at 320 °C over Fe/KA

	CO <sub>2</sub> conv. (%)	CO sel (%)	Selectivity of hydrocarbons (%)					O/P ratio
			CH <sub>4</sub> sel (%)	C <sub>2</sub> -C <sub>4</sub> paraffins sel (%)	C <sub>2</sub> -C <sub>4</sub> olefins sel (%)	C <sub>5+</sub> olefins (sel %)	C <sub>5+</sub> (sel %)	
DAC	22.4	<5	79.7	8.9	11.4	0.0	0.0	1.3
CO <sub>2</sub> :H <sub>2</sub> = 1:10	22	54.7	33.5	33.1	24.2	9.21	0.0	0.73
CO <sub>2</sub> :H <sub>2</sub> = 1:3	9.55	79.4	33.4	22.5	36.6	6.91	0.50	1.62

Fe/KA = 2 g, amount of material: 2 g; pretreatment conditions: H<sub>2</sub> = 60 mL min<sup>-1</sup>, 400 °C, 5 h; CO<sub>2</sub> capture conditions: CO<sub>2</sub> = 400 ppm in N<sub>2</sub> (flow rate = 1200 mL min<sup>-1</sup>), H<sub>2</sub>O vapor = 0.5 mol%, 25 °C, 4 h; hydrogenation: H<sub>2</sub> = 60 mL min<sup>-1</sup>, 1.0 MPa, 320 °C for 2.5 h (5 °C min<sup>-1</sup>); CO<sub>2</sub>:H<sub>2</sub> = 1:10 or 1:3 ratio; flow rate = 60 mL min<sup>-1</sup>, 1.0 MPa, 320 °C for 2.5 h (5 °C min<sup>-1</sup>); GHSV = 1800 mL h<sup>-1</sup> g<sup>-1</sup>.



**Table 4** Comparison of hydrogenation of gas-phase CO<sub>2</sub> at 360 °C over Fe/KA

	CO <sub>2</sub> conv. (%)	CO sel (%)	Selectivity of hydrocarbons (%)					O/P ratio
			CH <sub>4</sub> sel (%)	C <sub>2</sub> –C <sub>4</sub> paraffins sel (%)	C <sub>2</sub> –C <sub>4</sub> olefins sel (%)	C <sub>5</sub> + olefins (sel %)	C <sub>5</sub> + (sel %)	
CO <sub>2</sub> : H <sub>2</sub> = 1 : 10	66.0	11.5	49.5	8.19	36.4	5.27	0.61	4.5
CO <sub>2</sub> : H <sub>2</sub> = 1 : 3	14.7	37.3	34.4	6.97	48.0	9.17	1.40	6.9

Fe/KA = 2 g, pretreatment conditions: H<sub>2</sub> = 60 mL min<sup>−1</sup>, 400 °C, 5 h; CO<sub>2</sub> : H<sub>2</sub> = 1 : 10 or 1 : 3 ratio; flow rate = 60 mL min<sup>−1</sup>, 1.0 MPa, 320 °C for 2.5 h (5 °C min<sup>−1</sup>) followed by heating to 360 °C (5 °C min<sup>−1</sup>) for 2 h; GHSV = 1800 mL h<sup>−1</sup> g<sup>−1</sup>.

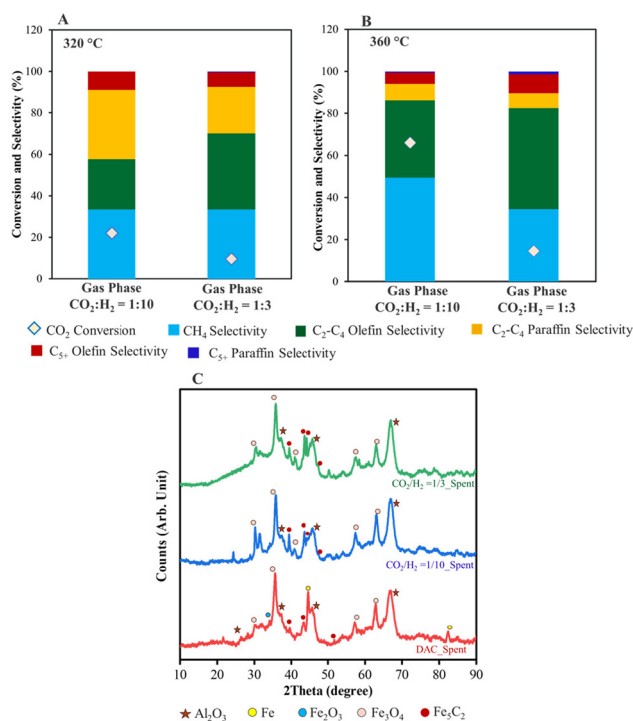


**Fig. 6** Comparison of gas-phase hydrogenation at (A) 320 °C and (B) 360 °C using Fe/KA. (C) Comparison of XRD of Fe/KA for DAC and gas-phase reactions carried out at 1 : 10 and 1 : 3 ratios of CO<sub>2</sub> : H<sub>2</sub>. Reaction Conditions: Fe/KA: 2 g, total flow rate = 60 mL min<sup>−1</sup>, CO<sub>2</sub> : H<sub>2</sub> = 1 : 10 or 1 : 3 ratios; flow rate = 60 mL min<sup>−1</sup>, 1.0 MPa, 320 °C for 2.5 h (5 °C min<sup>−1</sup>), followed by heating to 360 °C for 2 h (5 °C min<sup>−1</sup>); GHSV = 1800 mL h<sup>−1</sup> g<sup>−1</sup>.

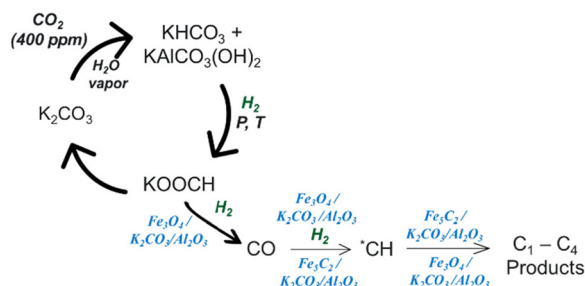
The XRD spectra of the spent DAC and gas-phase CO<sub>2</sub> hydrogenation materials are shown in Fig. 6C. Fe<sub>3</sub>O<sub>4</sub> was observed in all spent materials. The Fe<sub>5</sub>C<sub>2</sub> diffraction patterns are more pronounced for the 1 : 3 CO<sub>2</sub>/H<sub>2</sub> reaction compared to the 1 : 10 CO<sub>2</sub>/H<sub>2</sub> reaction. This agrees with the decreased CH<sub>4</sub> selectivity and increased O/P ratio of the 1 : 3 CO<sub>2</sub>/H<sub>2</sub> reaction because both Fe<sub>3</sub>O<sub>4</sub> (for the RWGS) and Fe<sub>5</sub>C<sub>2</sub> are important for C–C formation (Table 4). Peaks for Fe were also observed in the spent DAC material, showing that not all of the Fe was carburized to Fe<sub>5</sub>C<sub>2</sub>. The formation of the carbide-phase reaction route is as follows: Fe<sub>2</sub>O<sub>3</sub> → Fe<sub>3</sub>O<sub>4</sub> → FeO → Fe, and then finally the Fe is carburized to Fe<sub>5</sub>C<sub>2</sub>.<sup>63</sup>

The Fourier transform infrared spectroscopy (FTIR) spectrum of the spent DAC and gas-phase CO<sub>2</sub> hydrogenation materials were compared (Fig. S6†). The C–H vibrations were seen between 2960–2627 cm<sup>−1</sup> corresponding to formate and other bound –CH species. The carbonyl vibration of formate was observed at the ~1631 cm<sup>−1</sup> region.<sup>64</sup> The Fe–CO interactions were visible in the 1800–2100 cm<sup>−1</sup> region, which corresponds to bound CO with different forms of Fe.<sup>65</sup> In addition to formate and CO, there are additional bands visible for carbonates and bicarbonates in the IR spectrum.

To further enhance the formation of C–C coupled products, we pretreated the Fe/KA with an H<sub>2</sub>/CO gas mixture to improve iron carbide formation. The outlet gas stream during the pretreatment consisted of CO<sub>2</sub>, CH<sub>4</sub> and C<sub>2</sub>–C<sub>4</sub> hydrocarbons. After H<sub>2</sub>/CO pretreatment, Fe/KA was treated with H<sub>2</sub> at 400 °C to remove CO<sub>2</sub> and other hydrocarbons adsorbed on the Fe/KA prior to CO<sub>2</sub> capture. The capture capacity of this H<sub>2</sub>/CO pretreated Fe/KA was 1659 μmol g<sup>−1</sup> at our standard CO<sub>2</sub> capture conditions, which is comparable to Fe/KA (Table 2). Subsequent hydrogenation of the captured CO<sub>2</sub> resulted in an enhancement in C–C coupled products selectivity to 27.9% (16.7% selectivity to C<sub>2</sub>–C<sub>4</sub> olefins and 11.2% selectivity to C<sub>2</sub>–C<sub>4</sub> paraffins) with a slight improvement in the CO<sub>2</sub> conversion to 24.5%. The selectivity of the hydrogenated products for the first hour at 320 °C is shown in Fig. S7.† It is evident that the selectivity to C–C coupled products was high, ~50% (with >30% selectivity to C<sub>2</sub>–C<sub>4</sub> olefins), initially, but decreased significantly as the concentration of the captured CO<sub>2</sub> decreased.

Based on the selectivity of the products and the XRD and FTIR analyses of the spent samples, the conversion of captured CO<sub>2</sub> to olefins occurs through the direct CO<sub>2</sub> conversion pathway, where the CO<sub>2</sub> is converted to CO *via* the RWGS in the presence of Fe<sub>3</sub>O<sub>4</sub>.<sup>66</sup> Subsequently, the CO is converted to C–C products following the FTS mechanism in the presence of Fe<sub>5</sub>C<sub>2</sub>.<sup>66</sup> A proposed pathway has been shown in Scheme 1. When CO<sub>2</sub> (400 ppm) is captured in the presence of water vapor at room temperature, the K<sub>2</sub>CO<sub>3</sub> of Fe/KA transforms into KHCO<sub>3</sub> and KAlCO<sub>3</sub>(OH)<sub>2</sub>. This transformation leads to the formation of HCOOK and CO upon hydrogenation catalyzed by Fe<sub>3</sub>O<sub>4</sub>/KA. The Fe<sub>3</sub>O<sub>4</sub>/KA is derived from Fe<sub>2</sub>O<sub>3</sub>/KA in the presence of H<sub>2</sub>. Furthermore, the Fe<sub>3</sub>O<sub>4</sub>/KA facilitates the conversion of CO to \*CH species, which undergo C–C coupling in the presence of Fe<sub>5</sub>C<sub>2</sub> formed *in situ* during the reaction. The increased selectivity observed for the C–C coupled pro-





**Scheme 1** Proposed mechanism for the conversion of captured CO<sub>2</sub> to C–C coupled products in the presence of Fe/KA.

ducts (as depicted in Table 2 and Fig. S7†) following the pretreatment of Fe/KA with H<sub>2</sub>/CO gas mixture strongly suggests that the enhanced formation of Fe<sub>5</sub>C<sub>2</sub> facilitates C–C coupling.

A preliminary techno-economic analysis (TEA) and life-cycle analysis (LCA) were conducted to evaluate the proposed iDAC-CAT technology for olefins production. In both TEA and LCA, it was assumed that renewable hydrogen, electri-

**Table 5** Technology performance measures and assumptions for TEA and LCA

Assumptions	Value	Assumptions	Value
Adsorption temperature (°C)	25	Conversion temperature (°C)	320
Adsorption pressure (bar)	1	Conversion pressure (bar)	10
Adsorption time (hr)	2	Conversion time with heating (hr)	2
CO <sub>2</sub> capture (%)	62	CO <sub>2</sub> conversion (%)	80
Sorbent loading (wt% CO <sub>2</sub> )	5	C <sub>2+</sub> olefin selectivity (%)	60
Plant size (tonne CO <sub>2</sub> per year)	100 000	CH <sub>4</sub> selectivity (%)	40
H <sub>2</sub> Price (\$ per kg)	5	Excess hydrogen (ratio over stoic)	4

city, and fossil-based natural gas were used as main energy inputs. A process model was developed in Aspen Plus V14 to calculate the mass and energy balance and life-cycle inventory of the proposed technology based on the performance measures and assumptions listed in Table 5. The results were compared with NETL's case study for sorbent-based DAC<sup>67</sup> and other CO<sub>2</sub> to olefin technologies available in the literature.<sup>68</sup>

Fig. 7 shows the process flow diagram of the technology, where air first enters the adsorption bed, and CO<sub>2</sub> is adsorbed by the sorbent at ambient conditions. The bed is then heated to 320 °C and H<sub>2</sub> is fed to the bed to produce CH<sub>4</sub> and olefins from CO<sub>2</sub>. The product stream leaving the adsorption bed contains H<sub>2</sub>, CH<sub>4</sub>, and C<sub>2+</sub> olefins. H<sub>2</sub> is first separated in the pressure swing adsorption (PSA) unit. The remaining products are then sent to a de-methanization tower. This tower is of the design commonly used in the commercial ethylene plants, and operated at cryogenic conditions (–100 °C, 35 bar). The CH<sub>4</sub> and C<sub>2+</sub> olefin streams from the tower are depressurized and then used to pre-chill the inlet stream. In the TEA, the plant size was set the same as Case 0B in the NETL's case study for sorbent-based DAC.<sup>67</sup> The capital cost of the iDAC-CAT unit was calculated by adjusting NETL Case 0B value<sup>67</sup> based on flowrate and cycling time. The capital cost of the downstream product separation and purification section was calculated using Aspen Process Economic Analyzer V14. A simple annualized cost approach was used to calculate the minimum olefin selling price with 20-year depreciation and 10% per year return on investment. It was assumed that the renewable natural gas (RNG) produced as by-product can be sold at a price of \$13 per MMBtu,<sup>69</sup> roughly five times of the market price of fossil-based natural gas. For the Fe/KA material, CatCost™ tool<sup>70</sup> was used to estimate its production cost as a pre-commercial material as well as the utility consumptions and emissions during the manufacturing step. For the LCA, a cradle-to-gate system boundary was used to evaluate the life-cycle greenhouse gases (GHG) emissions of olefin production using the iDAC-CAT technology, which was compared with conventional petrochemical process. The functional unit

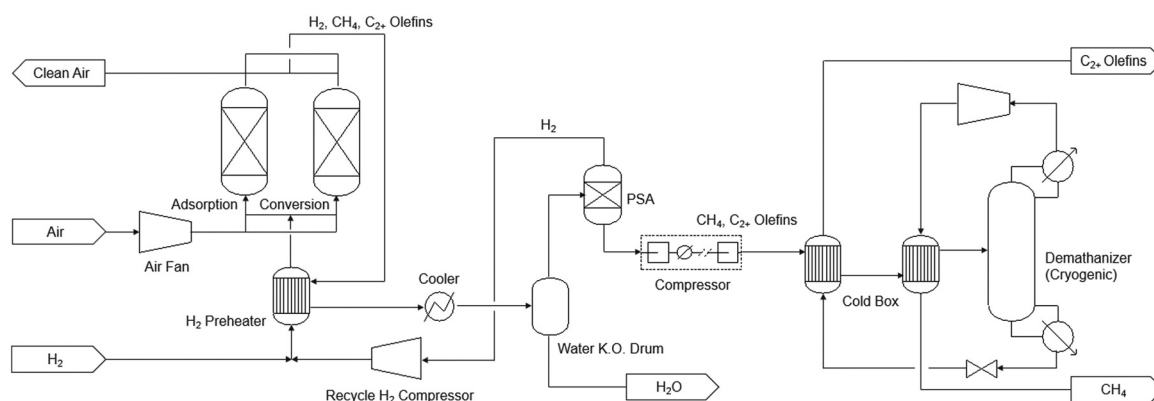


**Fig. 7** Process flow diagram of the proposed integrated DAC-CAT technology for olefins production.





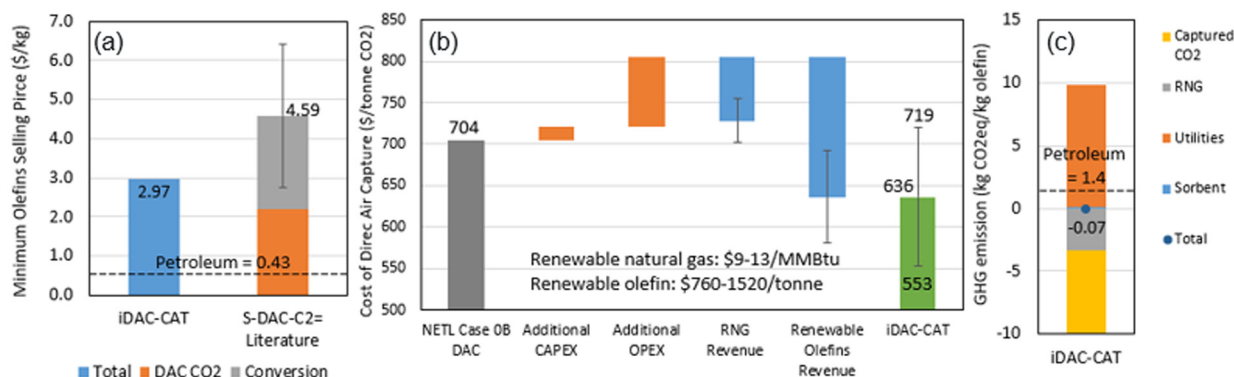


Fig. 8 Economic and environmental performance: (a) minimum olefin selling price; (b) cost of direct air capture; (c) life-cycle GHG emissions.

Table 6 Mass and Energy Balance and life-cycle inventory for the iDAC-CAT process

	Mass energy balance	Life cycle inventory	Carbon intensity
Products			
C <sub>2+</sub> olefins	2360 kg h <sup>-1</sup>		
RNG	2015 kg h <sup>-1</sup>	−0.045 MMBtu kg <sup>-1</sup> C <sub>2+</sub> olefins	72.62 kg CO <sub>2</sub> eq. MMBtu <sup>-1</sup> NG
Feedstock			
Renewable H <sub>2</sub>	2112 kg h <sup>-1</sup>	0.895 kg kg <sup>-1</sup> C <sub>2+</sub> olefins	0 kg CO <sub>2</sub> eq. kg <sup>-1</sup> H <sub>2</sub>
CO <sub>2</sub> captured	15 553 kg h <sup>-1</sup>	6.590 kg kg <sup>-1</sup> C <sub>2+</sub> olefins	−1 kg CO <sub>2</sub> eq. kg <sup>-1</sup> CO <sub>2</sub>
Sorbent (Fe/KA)	116 kg h <sup>-1</sup>	0.049 kg kg <sup>-1</sup> C <sub>2+</sub> olefins	2.20 kg CO <sub>2</sub> eq. kg <sup>-1</sup> sorbent
Utilities			
Electricity	32 984 kW	13.98 kW h kg <sup>-1</sup> C <sub>2+</sub> olefins	0 kg CO <sub>2</sub> eq. kW <sup>-1</sup> h <sup>-1</sup> electricity
NG	315.3 MMBtu h <sup>-1</sup>	0.133 MMBtu kg <sup>-1</sup> C <sub>2+</sub> olefins	72.62 kg CO <sub>2</sub> eq. MMBtu <sup>-1</sup> NG

was set to per kg of olefins produced. Carbon Intensity data for each raw material and energy involved in the process were sourced from the GREET 2022<sup>71</sup> and Ecoinvent V3.8 databases.

The preliminary TEA and LCA results were summarized in Fig. 8, while the mass and energy balance, life-cycle inventory and carbon intensity were provided in Table 6. Fig. 8(a) suggests the integrated iDAC-CAT technology can potentially produce renewable olefins at a cost 35% lower than that of a separated DAC and CO<sub>2</sub> to olefins (S-DAC-C<sub>2</sub>=) technology.<sup>67,68</sup> Fig. 8(b) indicates that the iDAC-CAT technology can significantly reduce the cost of DAC on a per tonne CO<sub>2</sub> basis. The error bars in both Fig. 8(a) and (b) represent the uncertainties in TEA results from literature, as well as the market prices of RNG and olefins. Furthermore, Fig. 8(c) and Table 6 demonstrate that the CO<sub>2</sub> adsorbed from the atmosphere and the GHG emissions avoided by producing RNG can completely offset the GHG emissions from upstream processes and the iDAC-CAT process when renewable H<sub>2</sub> is used as a process input. A GHG emission reduction of 105% can be achieved compared to the petroleum baseline.

## Conclusions

A series of materials have been evaluated for direct air capture and conversion to C–C coupled products for the first time. A novel multifunctional and multicomponent material for

iDAC-CAT has been developed, employing a combination of non-noble metal and solid inorganic sorbent, Fe/K<sub>2</sub>CO<sub>3</sub>/Al<sub>2</sub>O<sub>3</sub>. Upon the impregnation of catalytic Fe particles to the sorbent (K<sub>2</sub>CO<sub>3</sub>/Al<sub>2</sub>O<sub>3</sub>), despite the decrease in surface area, pore size, and pore volume, high and consistent CO<sub>2</sub> capture was realized at room temperature in presence of water vapor. This shows that the addition of Fe particles did not significantly change the CO<sub>2</sub> capture property of K<sub>2</sub>CO<sub>3</sub>/Al<sub>2</sub>O<sub>3</sub>. On recycling, the material showed a consistent capture capacity of ~5 wt% for up to five cycles, followed by consistent CO<sub>2</sub> conversion into C–C products. In contrast, the physical mixture of Fe<sub>2</sub>O<sub>3</sub> and K<sub>2</sub>CO<sub>3</sub>/Al<sub>2</sub>O<sub>3</sub> desorbed the CO<sub>2</sub> and showed no formation of C<sub>1</sub>–C<sub>4</sub> products on hydrogenation. Based on this comparison and activity data of various combination of materials, along with XRD and BET results, it is evident that the proximity between the Fe and K on the Al<sub>2</sub>O<sub>3</sub> is important for CO<sub>2</sub> activation and subsequent conversion to C–C products.

We have successfully developed an approach for integrated direct air capture and conversion to C–C coupled products using Fe/K<sub>2</sub>CO<sub>3</sub>/Al<sub>2</sub>O<sub>3</sub>. The utilization of this material for CO<sub>2</sub> capture from the air and subsequent conversion to C<sub>2+</sub> products represents an environmentally friendly approach. Despite the current breakthrough and success of the bench-scale experiment, scaling up poses multiple risks. Factors such as kinetics, material mechanical strength and stability, environmental conditions throughout the year, processing temperature range, and deployment site must be carefully con-



sidered during the scaling process. Our preliminary TEA analysis indicates that iDAC-CAT technology has the potential to substantially decrease the cost of DAC. The preliminary LCA suggests a 105% reduction in GHG emissions compared to the petroleum baseline, and indicates a negative cradle-to-gate GHG emission for renewable olefin production *via* iDAC-CAT when renewable H<sub>2</sub> is used as the process input. Future efforts will focus on developing materials with enhanced reactivity for C–C coupling and stronger CO<sub>2</sub> binding affinity to prevent desorption during conversion at the high temperatures required for C–C coupling reactions. Further exploration of Fe/K<sub>2</sub>CO<sub>3</sub>/Al<sub>2</sub>O<sub>3</sub> under varying conditions, and experimentation with different material combinations, is needed to improve the conversion efficiency. This exploration should be accompanied by a full TEA and LCA to assess its feasibility for real-world applications.

## Author contributions

Shazia Sharmin Satter: investigation, data curation, and writing – original draft; Johnny Saavedra Lopez: investigation, methodology, and writing – editing; Michael L. Hubbard: investigation and data curation; Yuan Jiang: TEA, LCA and writing – editing; Robert A. Dagle: conceptualization, and writing – editing; Jotheeswari Kothandaraman: supervision, funding acquisition, conceptualization, investigation, data curation, and writing – review and editing.

## Conflicts of interest

There are no conflicts to declare.

## Acknowledgements

This work was supported by the Laboratory Directed Research and Development Program (LDRD) at Pacific Northwest National Laboratory (PNNL). The authors would like to thank Dr Jaelynn A. King and Dr Austin D. Winkelman for performing the FTIR and XRD measurements, respectively. The Pacific Northwest National Laboratory is proudly operated by Battelle for the US Department of Energy.

## References

- J. Hilaire, J. C. Minx, M. W. Callaghan, J. Edmonds, G. Luderer, G. F. Nemet, J. Rogelj and M. del Mar Zamora, *Clim. Change*, 2019, **157**, 189–219.
- W. J. Shaw, M. K. Kidder, S. R. Bare, M. Delferro, J. R. Morris, F. M. Toma, S. D. Senanayake, T. Autrey, E. J. Biddinger, S. Boettcher, M. E. Bowden, P. F. Britt, R. C. Brown, R. M. Bullock, J. G. Chen, C. Daniel, P. K. Dorhout, R. A. Efroymsen, K. J. Gaffney, L. Gagliardi, A. S. Harper, D. J. Heldebrant, O. R. Luca, M. Lyubovsky, J. L. Male, D. J. Miller, T. Prozorov, R. Rallo, R. Rana, R. M. Rioux, A. D. Sadow, J. A. Schaidle, L. A. Schulte, W. A. Tarpeh, D. G. Vlachos, B. D. Vogt, R. S. Weber, J. Y. Yang, E. Arenholz, B. A. Helms, W. Huang, J. L. Jordahl, C. Karakaya, K. C. Kian, J. Kothandaraman, J. Lercher, P. Liu, D. Malhotra, K. T. Mueller, C. P. O'Brien, R. M. Palomino, L. Qi, J. A. Rodriguez, R. Rousseau, J. C. Russell, M. L. Sarazen, D. S. Sholl, E. A. Smith, M. B. Stevens, Y. Surendranath, C. J. Tassone, B. Tran, W. Tumas and K. S. Walton, *Nat. Rev. Chem.*, 2024, **8**, 376–400.
- P. M. Bhatt, Y. Belmabkhout, A. Cadiau, K. Adil, O. Shekhah, A. Shkurenko, L. J. Barbour and M. Eddaoudi, *J. Am. Chem. Soc.*, 2016, **138**, 9301–9307.
- D. G. Boer, J. Langerak and P. P. Pescarmona, *ACS Appl. Energy Mater.*, 2023, **6**, 2634–2656.
- P. Murge, S. Dinda and S. Roy, *Langmuir*, 2019, **35**, 14751–14760.
- R. V. Siriwardane, M.-S. Shen, E. P. Fisher and J. A. Poston, *Energy Fuels*, 2001, **15**, 279–284.
- S. A. Didas, S. Choi, W. Chaikittisilp and C. W. Jones, *Acc. Chem. Res.*, 2015, **48**, 2680–2687.
- W. Chaikittisilp, H.-J. Kim and C. W. Jones, *Energy Fuels*, 2011, **25**, 5528–5537.
- N. G. McQueen, K. V. McCormick, C. Blumanthal, K. Pisciotto and M. Wilcox, *J. Prog. Energy*, 2021, **3**, 032001.
- M. A. Sabri, S. Al Jitan, D. Bahamon, L. F. Vega and G. Palmisano, *Sci. Total Environ.*, 2021, **790**, 148081.
- D. J. Heldebrant, J. Kothandaraman, N. M. Dowell and L. Brickett, *Chem. Sci.*, 2022, **13**, 6445–6456.
- R. E. Siegel, S. Pattanayak and L. A. Berben, *ACS Catal.*, 2022, **13**, 766–784.
- S. Kar, A. Goeppert and G. K. S. Prakash, *Acc. Chem. Res.*, 2019, **52**, 2892–2903.
- J. Kothandaraman, A. Goeppert, M. Czaun, G. A. Olah and G. K. Prakash, *J. Am. Chem. Soc.*, 2016, **138**, 778–781.
- N. M. Rezayee, C. A. Huff and M. S. Sanford, *J. Am. Chem. Soc.*, 2015, **137**, 1028–1031.
- J. B. Jakobsen, M. H. Ronne, K. Daasbjerg and T. Skrydstrup, *Angew. Chem., Int. Ed.*, 2021, **60**, 9174–9179.
- S. Kar, J. Kothandaraman, A. Goeppert and G. K. S. Prakash, *J. CO<sub>2</sub> Util.*, 2018, **23**, 212–218.
- X. Shi, H. Xiao, H. Azarabadi, J. Song, X. Wu, X. Chen and K. S. Lackner, *Angew. Chem., Int. Ed.*, 2020, **59**, 6984–7006.
- R. Custelcean, *Annu. Rev. Chem. Biomol. Eng.*, 2022, **13**, 217–234.
- J. Kothandaraman, J. S. Lopez, Y. Jiang, E. D. Walter, S. D. Burton, R. A. Dagle and D. J. Heldebrant, *Adv. Energy Mater.*, 2022, **12**(46), 2202369.
- J. Kothandaraman, J. S. Lopez, Y. Jiang, E. D. Walter, S. D. Burton, R. A. Dagle and D. J. Heldebrant, *ChemSusChem*, 2021, **14**, 4812–4819.
- J. Kothandaraman, A. Goeppert, M. Czaun, G. A. Olah and G. K. S. Prakash, *Green Chem.*, 2016, **18**, 5831–5838.
- D. Wei, H. Junge and M. Beller, *Chem. Sci.*, 2021, **12**, 6020–6024.



- 24 S. Jo, H. D. Son, T.-Y. Kim, J. H. Woo, D. Y. Ryu, J. C. Kim, S. C. Lee and K. L. Gilliard-AbdulAziz, *Chem. Eng. J.*, 2023, **469**, 143772.
- 25 T. Sasayama, F. Kosaka, Y. Liu, T. Yamaguchi, S.-Y. Chen, T. Mochizuki, A. Urakawa and K. Kuramoto, *J. CO<sub>2</sub> Util.*, 2022, **60**, 102049.
- 26 M. S. Duyar, M. A. A. Treviño and R. J. Farrauto, *Appl. Catal., B*, 2015, **168–169**, 370–376.
- 27 L. Hu and A. Urakawa, *J. CO<sub>2</sub> Util.*, 2018, **25**, 323–329.
- 28 M. Abdallah, Y. C. Y. Lin and R. Farrauto, *Appl. Catal., B*, 2023, **339**, 123105.
- 29 C. Jeong-Potter, M. Abdallah, C. Sanderson, M. Goldman, R. Gupta and R. Farrauto, *Appl. Catal., B*, 2022, **307**, 120990.
- 30 C. Jeong-Potter and R. Farrauto, *Appl. Catal., B*, 2021, **282**, 119416.
- 31 C. Jeong-Potter, M. A. Arellano-Treviño, W. W. McNeary, A. J. Hill, D. A. Ruddy and A. T. To, *EES Catal.*, 2024, **2**, 253–261.
- 32 J. Pazdera, E. Berger, J. A. Lercher and A. Jentys, *Catal. Commun.*, 2021, **159**, 106347.
- 33 J. Pazdera, D. Issayeva, J. Titus, R. Gläser, O. Deutschmann and A. Jentys, *ChemCatChem*, 2022, **14**, e202200620.
- 34 L. C. Wirner, F. Kosaka, T. Sasayama, Y. Liu, A. Urakawa and K. Kuramoto, *Chem. Eng. J.*, 2023, **470**, 144227.
- 35 A. Bermejo-López, B. Pereda-Ayo, J. A. González-Marcos and J. R. González-Velasco, *J. CO<sub>2</sub> Util.*, 2019, **34**, 576–587.
- 36 F. Kosaka, Y. Liu, S.-Y. Chen, T. Mochizuki, H. Takagi, A. Urakawa and K. Kuramoto, *ACS Sustainable Chem. Eng.*, 2021, **9**, 3452–3463.
- 37 S. C. Lee, H. J. Chae, S. J. Lee, B. Y. Choi, C. K. Yi, J. B. Lee, C. K. Ryu and J. C. Kim, *Environ. Sci. Technol.*, 2008, **42**, 2736–2741.
- 38 M. S. Cho, S. C. Lee, H. J. Chae, Y. M. Kwon, J. B. Lee and J. C. Kim, *Process Saf. Environ. Prot.*, 2018, **117**, 296–306.
- 39 S. B. Jo, S. C. Lee, H. J. Chae, M. S. Cho, J. B. Lee, J.-I. Baek and J. C. Kim, *Korean J. Chem. Eng.*, 2016, **33**, 3207–3215.
- 40 J. Holladay, Z. Abdullah and J. Heyne, *Technical Report: Sustainable Aviation Fuel: Review of Technical Pathways, United States*, 2020, doi: DOI: [10.2172/1660415](https://doi.org/10.2172/1660415).
- 41 E. S. Sanz-Perez, C. R. Murdock, S. A. Didas and C. W. Jones, *Chem. Rev.*, 2016, **116**, 11840–11876.
- 42 J. Wang, L. Huang, R. Yang, Z. Zhang, J. G. Wu, Y. Gao, Q. Wang, D. O'Hare and Z. Zhong, *Energy Environ. Sci.*, 2014, **7**, 3478–3518.
- 43 J. V. Veselovskaya, V. S. Derevschikov, T. Y. Kardash and A. G. Okunev, *Renew. Bioresour.*, 2015, **3**, 1.
- 44 J. V. Veselovskaya, V. S. Derevschikov, T. Y. Kardash, O. A. Stonkus, T. A. Trubitsina and A. G. Okunev, *Int. J. Greenhouse Gas Control*, 2013, **17**, 332–340.
- 45 A. G. Okunev, V. E. Sharonov, Y. I. Aristov and V. N. Parmon, *React. Kinet. Catal. Lett.*, 2000, **71**, 355–362.
- 46 V. E. Sharonov, E. A. Tyshchishchin, E. M. Moroz, A. G. Okunev and Y. I. Aristov, *Russ. J. Appl. Chem.*, 2001, **74**, 409–413.
- 47 J. V. Veselovskaya, V. S. Derevschikov, A. S. Shalygin and D. A. Yatsenko, *Microporous Mesoporous Mater.*, 2021, **310**, 110624.
- 48 M. Yan, Y. Zhang, Q. Huan, Y. Song, X. Zhou, H. Wibowo and C. Yu, *Biomass Convers. Biorefin.*, 2022, **14**, 3667–3677.
- 49 N. Masoud, G. Bordanaba-Florit, T. v. Haasterecht and J. H. Bitter, *Ind. Eng. Chem. Res.*, 2021, **60**, 13749–13755.
- 50 C. Zhao, X. Chen and C. Zhao, *Energy Fuels*, 2009, **23**, 4683–4687.
- 51 S. C. Lee, H. J. Chae, B. Y. Choi, S. Y. Jung, C. Y. Ryu, J. J. Park, J.-I. Baek, C. K. Ryu and J. C. Kim, *Korean J. Chem. Eng.*, 2011, **28**, 480–486.
- 52 J. V. Veselovskaya, A. I. Lysikov, O. V. Netskina, D. V. Kuleshov and A. G. Okunev, *Ind. Eng. Chem. Res.*, 2020, **59**, 7130–7139.
- 53 J. Kothandaraman, J. S. Lopez, Y. Jiang, E. D. Walter, S. D. Burton, R. A. Dagle and D. J. Heldebrant, *Adv. Energy Mater.*, 2022, **12**, 2202369.
- 54 D. Wang, Z. H. Xie, M. D. Porosoff and J. G. G. Chen, *Chem*, 2021, **7**, 2277–2311.
- 55 T. Numpilai, N. Chanlek, Y. Poo-Arporn, C. K. Cheng, N. Siri-Nguan, T. Sornchamni, M. Chareonpanich, P. Kongkachuichay, N. Yigit, G. Rupprechter, J. W. Limtrakul and T. Wittoon, *ChemCatChem*, 2020, **12**, 3306–3320.
- 56 A. Ramirez, S. Ould-Chikh, L. Gevers, A. D. Chowdhury, E. Abou-Hamad, A. Aguilar-Tapia, J. L. Hazemann, N. Wehbe, A. J. Al Abdulghani, S. M. Kozlov, L. Cavallo and J. Gascon, *ChemCatChem*, 2019, **11**, 2879–2886.
- 57 Y. Han, C. Fang, X. Ji, J. Wei, Q. Ge and J. Sun, *ACS Catal.*, 2020, **10**, 12098–12108.
- 58 C. G. Visconti, M. Martinelli, L. Falbo, A. Infantes-Molina, L. Lietti, P. Forzatti, G. Iaquaniello, E. Palo, B. Picutti and F. Brignoli, *Appl. Catal., B*, 2017, **200**, 530–542.
- 59 H. Yu, C. Wang, T. Lin, Y. An, Y. Wang, Q. Chang, F. Yu, Y. Wei, F. Sun, Z. Jiang, S. Li, Y. Sun and L. Zhong, *Nat. Commun.*, 2022, **13**, 5987.
- 60 J. Ren, N. Ai, D. Ou and Y. Yu, *Mol. Catal.*, 2023, **538**, 112990.
- 61 H. M. T. Galvis and K. P. de Jong, *ACS Catal.*, 2013, **3**, 2130–2149.
- 62 J. Zieliński, I. Zglinicka, L. Znak and Z. Kaszukur, *Appl. Catal., A*, 2010, **381**, 191–196.
- 63 V. V. Ordonsky, B. Legras, K. Cheng, S. Paul and A. Y. Khodakov, *Catal. Sci. Technol.*, 2015, **5**, 1433–1437.
- 64 J. Lee and J. Otomo, *Ind. Eng. Chem. Res.*, 2023, **62**, 12096–12108.
- 65 V. I. Bogdan, A. E. Koklin, A. L. Kustov, Y. A. Pokusaeva, T. V. Bogdan and L. M. Kustov, *Molecules*, 2021, **26**, 2883.
- 66 B. Pawelec, R. Guil-Lopez, N. Mota, J. L. G. Fierro and R. M. Navarro Yerga, *Materials*, 2021, **14**, 6952.
- 67 J. Valentine and A. Zoelle, Direct Air Capture Case Studies: Sorbent System, DOE/NETL-2021/2865, National Energy Technology Laboratory, 2022, DOI: [10.2172/1879535](https://doi.org/10.2172/1879535).
- 68 A. Somoza-Tornos, O. J. Guerra, A. M. Crow, W. A. Smith and B. M. Hodge, *iScience*, 2021, **24**, 102813.





- 69 R. Gupta, Reactive CO<sub>2</sub> Capture DAC-DFM, *ARPA-E Reactive Carbon Capture Workshop*, 2022.
- 70 <https://catcost.chemcatbio.org/home>.
- 71 M. Wang, A. Elgowainy, U. Lee, K. H. Baek, A. Bafana, P. T. Benavides, A. Burnham, H. Cai, V. Cappello, P. Chen, Y. Gan, U. R. Gracida-Alvarez, T. R. Hawkins, R. K. Iyer, J. C. Kelly, T. Kim, S. Kumar, H. Kwon, K. Lee, X. Liu, Z. Lu, F. H. Masum, C. Ng, L. Ou, K. Reddi, N. Siddique, P. Sun, P. Vyawahare, H. Xu and G. G. Zaines, *Summary of Expansions and Updates in GREET® 2022*, ANL/ESIA-22/1, Argonne National Laboratory, 2022.

